



Research article

New sulfonated covalent organic framework for highly effective As(III) removal from water

Mohammad Khosravani^a, Mohsen Dehghani Ghanatghehstani^{a, **},
Farid Moeinpour^{b, *}, Hossein Parvaresh^a

^a Department of Environment, Faculty of Natural Resources, Bandar Abbas Branch, Islamic Azad University, Bandar Abbas, Iran

^b Department of Chemistry, Bandar Abbas Branch, Islamic Azad University, Bandar Abbas, 7915893144, Iran

ARTICLE INFO

Keywords:

Covalent organic frameworks
Adsorption
As(III)
Removal
Aqueous solutions

ABSTRACT

The goal of taking out As(III) from water is to reduce the detriment that poisonous metals can do to people and nature. A substance that can absorb As(III), TFPOTDB-SO₃H, was made by combining 2,5-diaminobenzenesulfonic acid and 2,4,6-tris-(4-formylphenoxy)-1,3,5-triazine in a reaction that joins molecules together. This substance can adsorb As(III) very well and has excellent qualities like being easy to use again, separate substances, and filter out liquids. At pH = 8 and at room temperature, TFPOTDB-SO₃H adsorbed a lot of As(III). It achieved a removal rate of 97.1 % within 10 min and could adsorb up to 344.8 mg/g. A research was conducted to investigate the effect of co-existing anions on the elimination of arsenic. The findings indicated that the presence of anions had a minimal adverse impact, reducing As(III) uptake by approximately 1–7 %. The kinetics of the uptake process were found to be controlled by the quasi-second order kinetic model, while the Langmuir isotherm model validated that the mechanism for As(III) removal was monolayer chemisorption. According to the thermodynamic analysis, the adsorption process was endothermic and occurred spontaneously. Moreover, even after 4 successive adsorption-desorption cycles, the adsorbent preserved a substantial uptake productivity of 88.86 % for As(III). The results collectively indicate that TFPOTDB-SO₃H holds considerable promise for the efficient adsorption and elimination of As(III) ions from wastewater.

1. Introduction

Water contamination is a significant global issue leading to numerous deaths [1]. The escalation in energy generation and the expanded utilization of heavy metals in industrial activities have led to an increased human contact with harmful elements. Specific transition metals, such as chromium, cadmium, arsenic, mercury, and lead are of particular concern due to their harmful impacts on human health, which include damage to organs, birth anomalies, and properties that can cause cancer [2]. To protect the environment and human well-being, it is crucial to find cost-effective and energy-efficient methods for removing trace contaminants from water [3]. Inorganic arsenic is a particularly problematic groundwater pollutant due to its high toxicity and ability to spread under various conditions. Approximately 140 million people are estimated to be exposed to this chemical, putting them at risk of developing lung, skin, bladder cancer [4]. Current market solutions for the remediation of heavy metals, including chemical precipitation, membranes,

* Corresponding author.

** Corresponding author.

E-mail addresses: m.dehghani@iauba.ac.ir (M. Dehghani Ghanatghehstani), Fa.Moeinpour@iaua.ac.ir (F. Moeinpour).

and sorbents, possess a number of drawbacks, including high costs, low removal efficiency, challenging regeneration, fouling issues, and the generation of large amounts of chemical sludge. Among these methods, adsorption shows promise due to its affordability and ease of implementation [5]. However, traditional adsorbents like natural amorphous iron oxides [6] and amorphous carbon [7] have limited effectiveness. Artificial iron nanoparticles have been engineered to enhance the absorption of arsenic by enlarging the surface area [8], however, they present challenges in terms of recovery and regeneration, and they lack selectivity due to their heightened reactivity [9]. Consequently, researchers are focusing on designing new materials like MOFs [10,11], zeolites [12], MgO nanoflakes [13,14], polymers [15], and covalent organic frameworks (COFs) [16] to enhance arsenic removal from contaminated water.

Covalent organic frameworks, or COFs, represent a category of crystalline substances characterized by a porous configuration made up of organic elements linked through robust covalent connections [17]. COFs display strong chemical resilience in both water-based and organic settings, distinguishing them from metal-organic frameworks which typically show instability under moist and aqueous conditions [18,19]. Their distinct structural features, including a large surface area, adjustable pore dimensions, and outstanding stability, render them particularly suitable for use in water purification applications [20–23]. Different molecules can be added or changed to tailor and enhance COFs at the level of atoms, which enables exact manipulation of their physical and chemical attributes to boost the effectiveness of pollutant extraction and the treatment of wastewater [24–32]. Within the field of separation science, the utilization of COFs has largely been dependent on their π - π stacking interactions and innate hydrophobic traits. Adding different groups of atoms to the COF structure can greatly increase how well it adsorbs and separates substances. Li and his team created a COF compound with sulfonate groups (called $\text{Fe}_3\text{O}_4@\text{COF}(\text{TpBD})@\text{Au-MPS}$ nanocomposites) that was made to capture a type of antibiotics called fluoroquinolones [33]. Zhao and his team created a substance with sulfonic acid groups (called $\text{Ni}/\text{CTF-SO}_3\text{H}$) by changing a COF material made of triazine after making it. They then used this to separate carbendazim and thiabendazole more effectively in a variety of juices, vegetables, and fruits [34]. Changing COFs after making them can enhance how well they separate substances, but it requires a complex and lengthy method to make the substance. So, making COFs with different groups of atoms already in them can make the substance preparation easier. As a result, these materials show great potential as substances that can adsorb and measure how well metal ions are removed from water solutions.

In the conducted research, a porous COF, named TFPOTDB- SO_3H , was produced using a systematic design strategy. The COF incorporated sulfonic acid groups and N, O atoms, which were instrumental in its superior efficiency in arsenic removal. A pliant binding block and a triazine-derived monomer were used to construct TFPOTDB- SO_3H , which had a network structure that showed high resonance in the polymerization process. This distinctive structure facilitated the direct interaction of the lone pair electrons with arsenic species.

2. Experimental

2.1. Materials

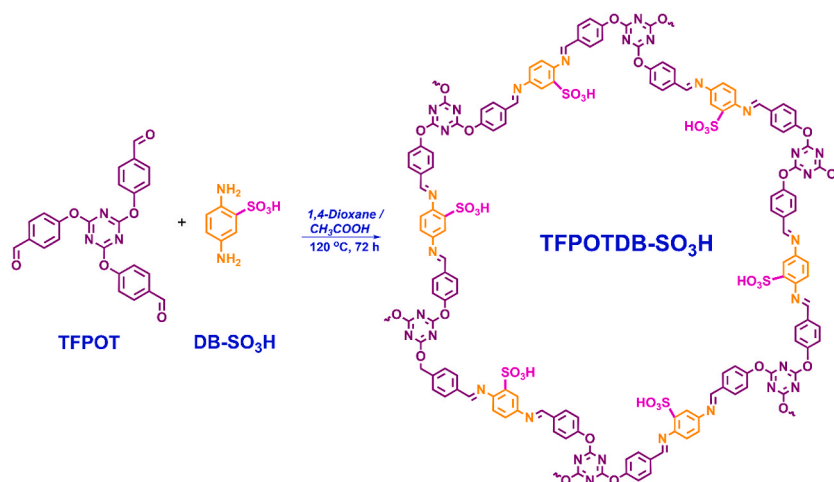
The experiment utilized chemicals procured from trading vendors without any further refinement. The special chemicals and their corresponding providers included: p-phenylenediamine sulfonic acid (DB- SO_3H) sourced from Sigma-Aldrich (with a purity of at least 97.0 %), glacial CH_3COOH also from Sigma-Aldrich (with a purity of at least 99 %), 1,4-dioxacyclohexane obtained from Merck, $\text{C}_2\text{H}_5\text{OH}$ procured from Alfa Aesar (with a purity between 94 and 96 %), 2-propanone from Alfa Aesar (with a purity of 99.5 %), and HNO_3 also from Alfa Aesar. Trichlorotriazine and p-hydroxy benzaldehyde were acquired from Merck. All mixtures were formulated using water that had been deionized. The creation of As(III) stock solutions involved the dissolution of NaAsO_2 salt in deionized water. To modify the pH of the solution as required, HNO_3 and NaOH , both with a concentration of 0.1 mol/L, were utilized.

2.2. Characterization of materials

A variety of analytical methods were employed in the experimental examination of the sample. We performed the scanning electron microscopy (SEM) using the HITACHI, S-4160 scanning electron microscope. The Philips CM 120 microscope was used for the analysis involving transmission electron microscopy (TEM). The Thermo Nicolet 370 instrument, a product of Thermo Fisher in the USA, was used to acquire ATR-FTIR spectra, with the measurements being recorded in the range of 400–4000 cm^{-1} , employing a resolution of 4 cm^{-1} and an average of 64 scans. The surface area and pore size distribution assessment were conducted using the Micromeritics TriStar II Series, GA 30093 instrument from the USA, where N_2 gas served as the adsorbate, and measurements were carried out at 77 K. The thermogravimetry analysis (TGA) involved heating the sample from ambient temperature to 800 °C at a rate of 10 °C min^{-1} under an N_2 atmosphere using the STA503 TA instrument. X-ray diffraction (XRD) patterns were obtained within the 2–80° range using CuK_α radiation and a Bruker instrument from Germany. Finally, atomic absorption spectroscopy (AAS) (PerkinElmer 2380-Waltham) was utilized to determine the remaining concentrations of As(III) present in the solution.

2.3. Production and refinement of TFPOT (2,4,6-tris-(4-formylphenoxy)-1,3,5-triazine)

Initially, p-hydroxy benzaldehyde and NaOH were dissolved in a round bottom flask containing a mixture of acetone and water. The flask was then cooled to 0 °C using an ice bath. Subsequently, cyanuric chloride dissolved in acetone was slowly added to the solution over a span of 60 min, resulting in the formation of a white solid. The reaction proceeded for 12 h at room temperature. Once the reaction was complete, the white solid was filtered, thoroughly washed with water, and subjected to recrystallization using ethanol. Finally, the product was dried in a vacuum oven at 80 °C, resulting in a pure final product with a yield of 92 % in the form of a



Scheme 1. A thorough approach to the synthesis of TFPOADB-SO₃H.

white solid [35].

2.4. Method for producing covalent organic frameworks with sulfonate linkages (TFPOADB-SO₃H)

A sulfonated covalent organic framework (TFPOADB-SO₃H) was synthesized using a solvothermal reaction. We obtained a homogeneous dispersion by mixing TFPOADB (132.42 mg, 0.3 mmol), DB-SO₃H (85 mg, 0.45 mmol), 1,4-dioxane (20 mL), and aqueous CH₃COOH (3 M, 2 mL) and applying ultrasonic waves (80 W, 15 min). The autoclave was used to heat this mixture for 72 h at 120 °C. A dark red brown solid was obtained, which was cleaned with ethanol, water, and ethanol sequentially, and then desiccated under vacuum at 50 °C for 12 h. The yield was impressive at 78 %.

2.5. Sequential adsorption trials conducted in batches

The adsorption experiments were conducted using a 250 mL Erlenmeyer flask. The flask contained varying initial concentrations of metal ions and specific amounts of TFPOADB-SO₃H, and the experiments were carried out at different times under non-continuous conditions. For the experiments involving As(III), solutions with desired concentrations were prepared by diluting a 1000 ppm As (III) solution. The removal procedures were studied to determine the optimal conditions by investigating the effects of pH (ranging from 2 to 10) and time (from 0.5 to 60 min). The initial concentration of As(III) ranged from 5.0 to 120 mg/L, while the dosage of the adsorbent was between 1.0 and 100 mg/100 mL. After achieving adsorption equilibrium, the mixture was filtered to separate the adsorbent, and the remaining filtrate was analyzed using AAS. Each experiment was repeated three times to ensure accuracy and reliability. The following mathematical formulas (1-2) were utilized to determine the efficiency of removal (% Removal) and the equilibrium adsorption capacity (q_e) for As(III):"

$$\% \text{ Removal} = \frac{C_0 - C_e}{C_0} \times 100 \quad (1)$$

$$q_e = \frac{(C_0 - C_e)V}{m} \quad (2)$$

At time t, the solution has an initial As(III) concentration of C₀ (mg/L) and a remaining As(III) concentration of C_t (mg/L). The adsorbent adsorbs an equilibrium amount of As(III) of q_e (mg/g) and leaves a remaining As(III) concentration of C_e (mg/L) in the solution at equilibrium. The adsorbent has a mass of m (g) and the As(III) solution has a volume of V (L).

2.6. A sequential procedure for the discriminative uptake of As(III)

The selective adsorption of As(III) ions was done using a conventional method. Several Erlenmeyer flasks with a capacity of 250 mL each containing 50 mL aqueous solution of 10 mg/L As(III) and containing PO₄³⁻, Cl⁻, SiO₃²⁻ and SO₄²⁻ respectively were prepared. The concentration of each substance was 10 ppm and a buffer solution was used to keep the pH at 8. A slurry was formed by adding 10.0 mg of TFPOADB-SO₃H to each solution. The slurry was then mixed for 10 min at room temperature. Filtration was used to remove the adsorbent from the mixture. The resulting filter was subjected to AAS analysis to measure the residual concentration of As (III).

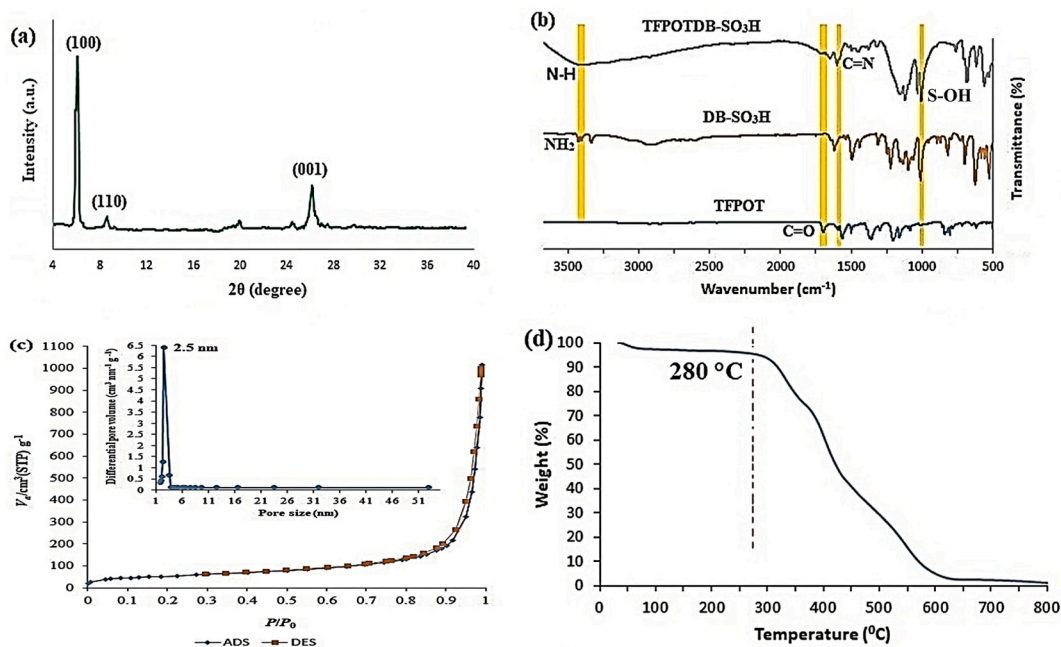


Fig. 1. (a) PXRD pattern of TFPO TDB-SO₃H, (b) FT-IR spectra of TFPO T, DB-SO₃H and TFPO TDB-SO₃H, (c) N₂ sorption isotherm and pore-size distribution of TFPO TDB-SO₃H and (d) TGA plot of TFPO TDB-SO₃H.

2.7. A comprehensive method for material reuse

Initially, a quantity of 10.0 mg of TFPO TDB-SO₃H was placed into a 250 mL Erlenmeyer flask. Following this, a 10-ppm solution (50 mL) was incorporated into the flask. The concoction was then agitated at ambient temperature for a duration of 10 min. Afterward, the mixture was strained using a piece of filter paper and cleansed with a 50 mL volume of water. The TFPO TDB-SO₃H material, which had adsorbed As(III) to its maximum capacity, was restored by immersing it in a 5 M NaCl solution for a duration of 2 h. Subsequently, the adsorbent underwent thorough rinsing with DI water multiple times until reached a neutral pH. Once all the salts were removed, the regenerated adsorbent was employed again in comparable adsorption processes, and this recycling procedure was carried out 4 times consecutively.

3. Results and discussion

3.1. Fabrication process of TFPO TDB-SO₃H

The solvothermal method was used to produce a covalent organic framework with sulfonic groups. The process entailed a Schiff-base condensation reaction involving *p*-phenylenediaminesulfonic acid (DB-SO₃H) and 2,4,6-tris-(4-formylphenoxy)-1,3,5-triazine (TFPO T). A catalyst of 3 M acetic acid was present to activate the aldehyde groups. The reaction was conducted at a temperature of 120 °C for a duration of 72 h in a 1,4-dioxane environment. Compared to the conventional vacuum solvothermal conditions, the method of synthesis is simpler and more accessible to users as shown in [Scheme 1](#).

3.2. Examinations via PXRD, FT-IR, BET, and TGA

The TFPO TDB-SO₃H adsorbent synthesis resulted in a dark red brown colored solid material. Its crystalline structure was confirmed by the powder X-ray diffraction (PXRD) method. [Fig. 1a](#) shows the PXRD pattern of TFPO TDB-SO₃H. The pattern has distinct peaks at 4.4°, 8.1°, and 25° that correspond to the facets (100), (110), and (001), respectively. The ordered structures of TFPO TDB-SO₃H in the covalent organic framework are revealed by these peaks, which are in line with the π - π stacking of the COF layers. The observation is confirmed by the peak of facet 001 in the PXRD spectrum [36]. The structure of TFPO TDB-SO₃H (shown in [Fig. 1b](#)) was confirmed by the FT-IR (Fourier transform infrared) spectroscopy results, which agreed with the PXRD findings. The FT-IR spectrum of the COF material lacked absorption peaks for the DB-SO₃H amine functional group and the TFPO T carbonyl functional group at approximately 3400 and 1700 cm⁻¹, respectively. On the other hand, a clear peak at 1005 cm⁻¹ for TFPO TDB-SO₃H showed the S-OH stretching mode of the -SO₃H unit [37]. The successful synthesis of the COF was confirmed by a new peak at 1621 cm⁻¹, which showed the imine condensation reaction. The successful synthesis of the framework material was suggested by these observations together [38,39]. N₂ sorption measurements at 77 K were used to study the porosity of the porous material. The results, shown in [Fig. 1c](#), displayed type I

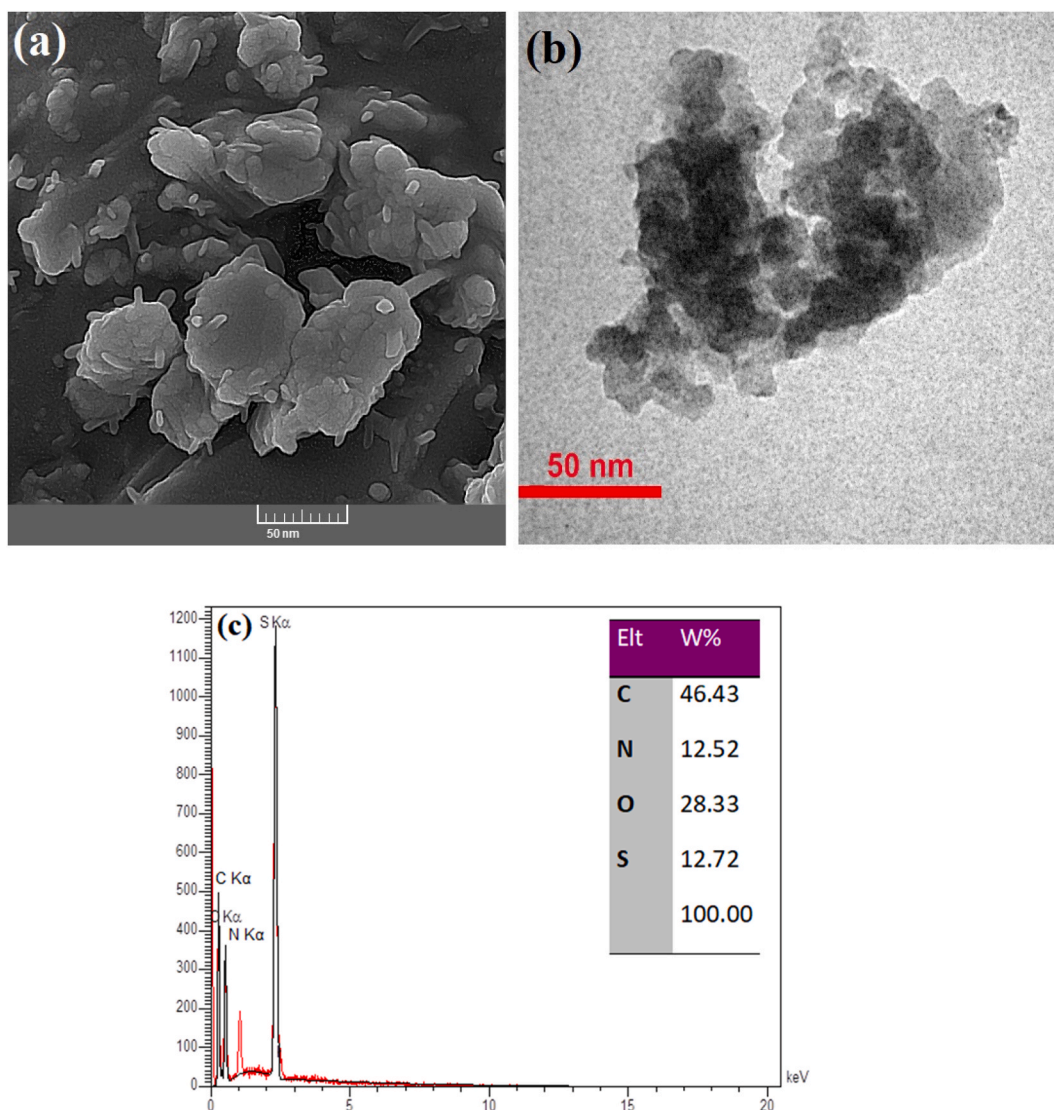


Fig. 2. SEM (a) and TEM (b) imaging of TFPOTDB-SO₃H, accompanied by EDS analysis results for TFPOTDB-SO₃H (c).

sorption isotherms. The surface area was calculated as 190.73 m²/g using the Brunauer–Emmett–Teller (BET) equation. Moreover, the Barrett–Joyner–Halenda (BJH) method was used to estimate the average pore diameter and pore volume from the adsorption branches. The values were about 2.5 nm for pore diameter and 1.55 cm³/g for pore volume. The stability of the adsorbent is essential for its real utilization. The thermal analysis conducted (Fig. 1 d) revealed that the TFPOTDB-SO₃H remained undamaged until reaching a temperature of 280 °C, indicating its impressive resistance to heat. At a temperature of 600 °C, it is likely that the imine bonds, as well as any other covalent bonds in the framework, are breaking down due to thermal decomposition. This is supported by research conducted by Altarawneh et al., which showed that COFs with imine bonds can be destroyed at temperatures higher than 400 °C [40]. Therefore, it is reasonable to assume that the complete destruction of the COF structure at 600 °C is due to thermal decomposition of its constituent bonds [41–43].

3.3. Analysis of data from SEM and TEM

SEM and TEM images of TFPOTDB-SO₃H are shown in Fig. 2 (a,b), respectively. The structure of the COF is made of spherical particles, as suggested by the SEM image. Additionally, the TEM image displays a flake and layered configuration which is likely due to hydrogen bonding between layers. The elemental analysis using energy-dispersive X-ray spectroscopy (EDS) is depicted in Fig. 2c, revealing the presence of sulfur in the COF called TFPOTDB-SO₃H. The image provides evidence of this. Additionally, it was determined that the percentage of sulfur in TFPOTDB-SO₃H is 12.72 %.

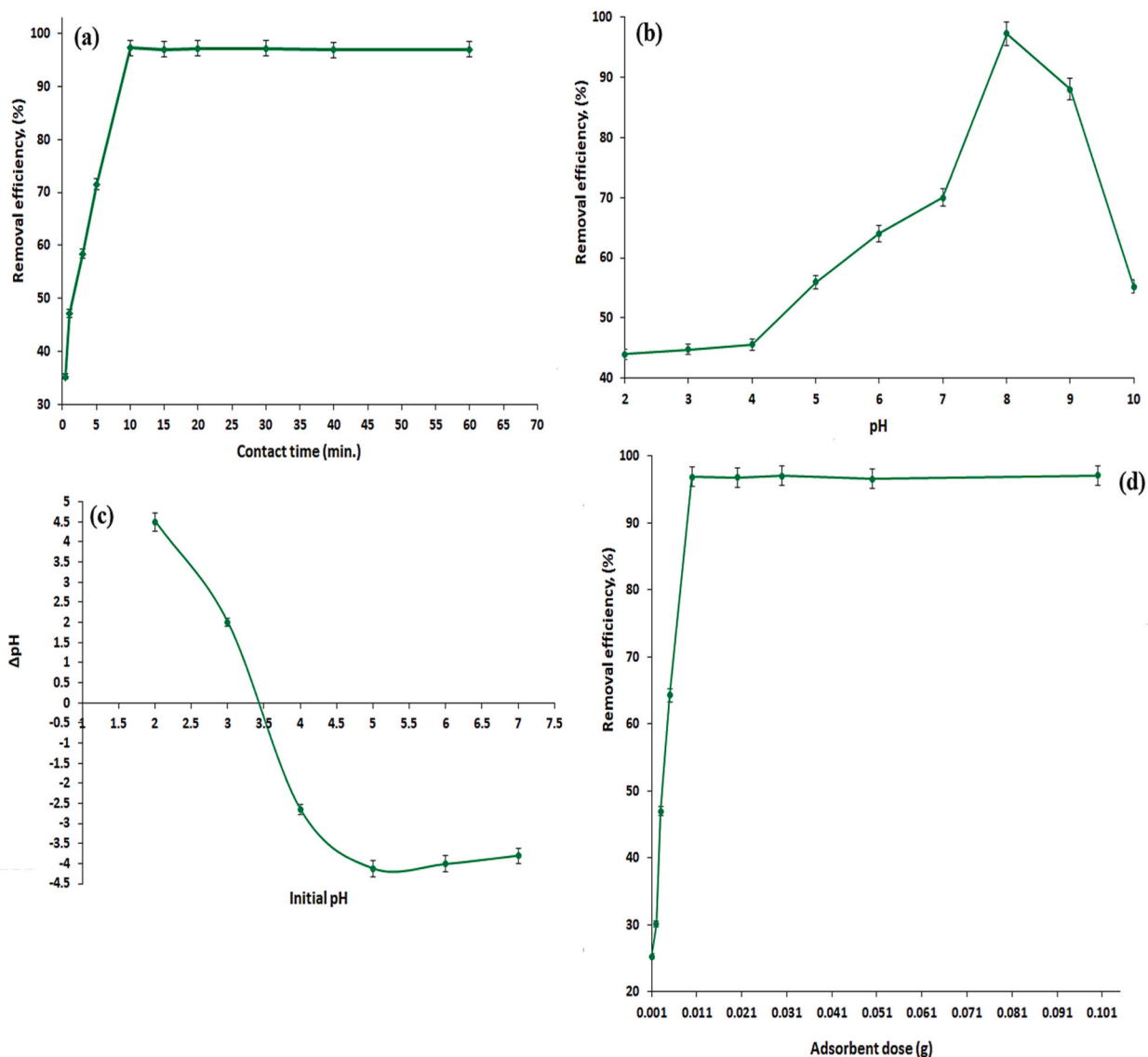


Fig. 3. Investigation of time-dependent As(III) removal efficiency by TFPOADB-SO₃H (a), evaluation of pH-dependence (b), establishing the pH_{PZC} of TFPOADB-SO₃H (c), evaluating the effect of adsorbent dosage on the removal of As(III) (d), impact of initial As(III) concentrations on the effectiveness of TFPOADB-SO₃H (e), regeneration of TFPOADB-SO₃H utilizing a 5 M NaCl solution (f).

3.4. As(III) removal

PXRD was used to check the water resistance of TFPOADB-SO₃H prior to the adsorption tests. The water-soaked TFPOADB-SO₃H samples and the original ones were compared using PXRD patterns after 24 h. The crystallinity of TFPOADB-SO₃H was maintained for both the non-immersed and the water-immersed samples. This finding validated the compounds' stability in water (Fig. S1).

The adsorption of As(III) was affected by the contact time, which was investigated utilizing the TFPOADB-SO₃H product (refer to Fig. 3a). The adsorption of As(III) was initially swift, achieving equilibrium in just 10 min. Beyond this point, no additional increase in As(III) adsorption was detected. The quick adsorption of As(III) in the early stages can be ascribed to the presence of many accessible surface sites on the TFPOADB-SO₃H substance. The level of pH is vital for the effective elimination of As(III). The pH of the solution and the point of zero charge (pH_{pzc}) of TFPOADB-SO₃H were considered to assess the impact of pH on the adsorption outcomes. Fig. 3b depicts how the pH influences the removal of As(III) ions using TFPOADB-SO₃H. The surface of TFPOADB-SO₃H shows a point of zero charge at 3.42 (refer to Fig. 3c), which implies that the surface charge is positive when the pH is less than 3.42 and negative when the pH exceeds 3.42. At pH values below 9.2, As(III) is present in its neutral form (H₃AsO₃), so neither attraction nor repulsion is possible. This suggests that other mechanisms, like surface complexation, may control the adsorption process [44]. The efficiency of As(III)

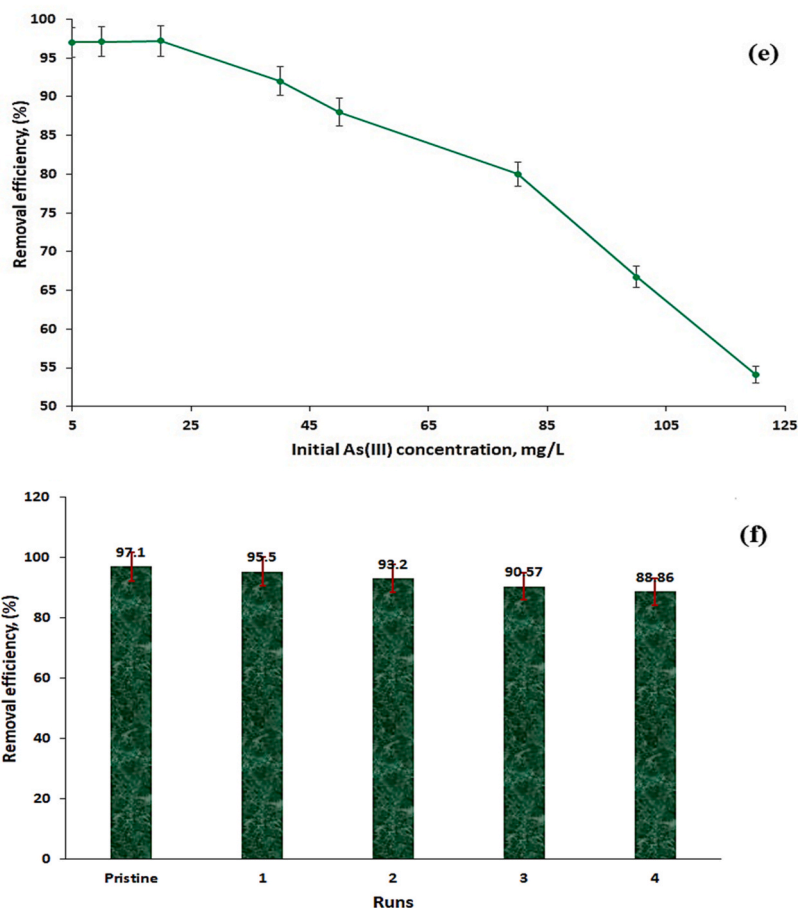


Fig. 3. (continued).

removal improved from a pH of 4 to approximately 8, but then decreased as the pH went above 8. The form of As(III) and the surface charges of the nanocomposites influenced the adsorption capacity and removal proficiency of As(III), which were optimal at a pH of 8. No electrostatic interaction can occur at this pH, where the TFPOADB-SO₃H is negatively charged and the As(III) is in its neutral form [45]. This trend has been seen previously [46–48]. However, at pH levels greater than 8, it undergoes a transformation into the negatively charged form known as H₂AsO₃⁻, as indicated by its pK_a values [49]. However, at pH levels above 8.0, electrostatic repulsion becomes significant, leading to reduce As(III) uptake at pH 10. This reduction in uptake can be ascribed to the negatively charged repulsion between the negative TFPOADB-SO₃H surface and the H₂AsO₃⁻ form of As(III), which predominates at pH 10. The maximum removal efficiency of 99.8 % was achieved at pH 8.0, which was determined as the optimal pH for TFPOADB-SO₃H in this study.

The optimal dosage of the adsorbent was determined by performing tests with different amounts of TFPOADB-SO₃H, from 1.0 to 100 mg/100 mL (refer to Fig. 3d). An increase in the amount of TFPOADB-SO₃H resulted in a proportional rise in the adsorption of As (III), due to the availability of more binding sites for the As(III) ions. The As(III) ions were removed by 99.56 % with just 10 mg/100 mL of TFPOADB-SO₃H. Further increases in dosage did not significantly affect the fraction of As(III) ions removed. The adsorption of As (III) by TFPOADB-SO₃H was examined at varying As(III) ion concentrations (from 5 to 120 mg/L), with the duration, pH, and TFPOADB-SO₃H dosage maintained at 10 min, 8.0, and 10 mg/100 mL, respectively. It was noted that the rate of As(III) adsorption declined from 97.0 % to 54.1 % as the As(III) concentration raised from 5 to 120 mg/L (refer to Fig. 3e). The reduction in uptake can be ascribed to the restricted number of uptake locations on the TFPOADB-SO₃H surface, resulting from the increased concentration of As (III) ions. In order to make adsorption more economically viable for practical applications, it's essential to minimize costs by discharging the adsorbed As(III) from TFPOADB-SO₃H and reproducing it. It was found that desorption was most productive in a 5 M NaCl solution. After 4 cycles of recycling, the TFPOADB-SO₃H only saw a minor reduction of 6.6 % in its adsorption capacity, demonstrating its superior regenerative ability (refer to Fig. 3f). TFPOADB-SO₃H is regarded as a cheap and effective adsorbent for eliminating As(III) from contaminated wastewater.

3.5. As(III) adsorption kinetics

Various kinetic models, including the pseudo-first-order model (Eq. (3)), pseudo-second-order model (Eq. (4)) and Elovich model

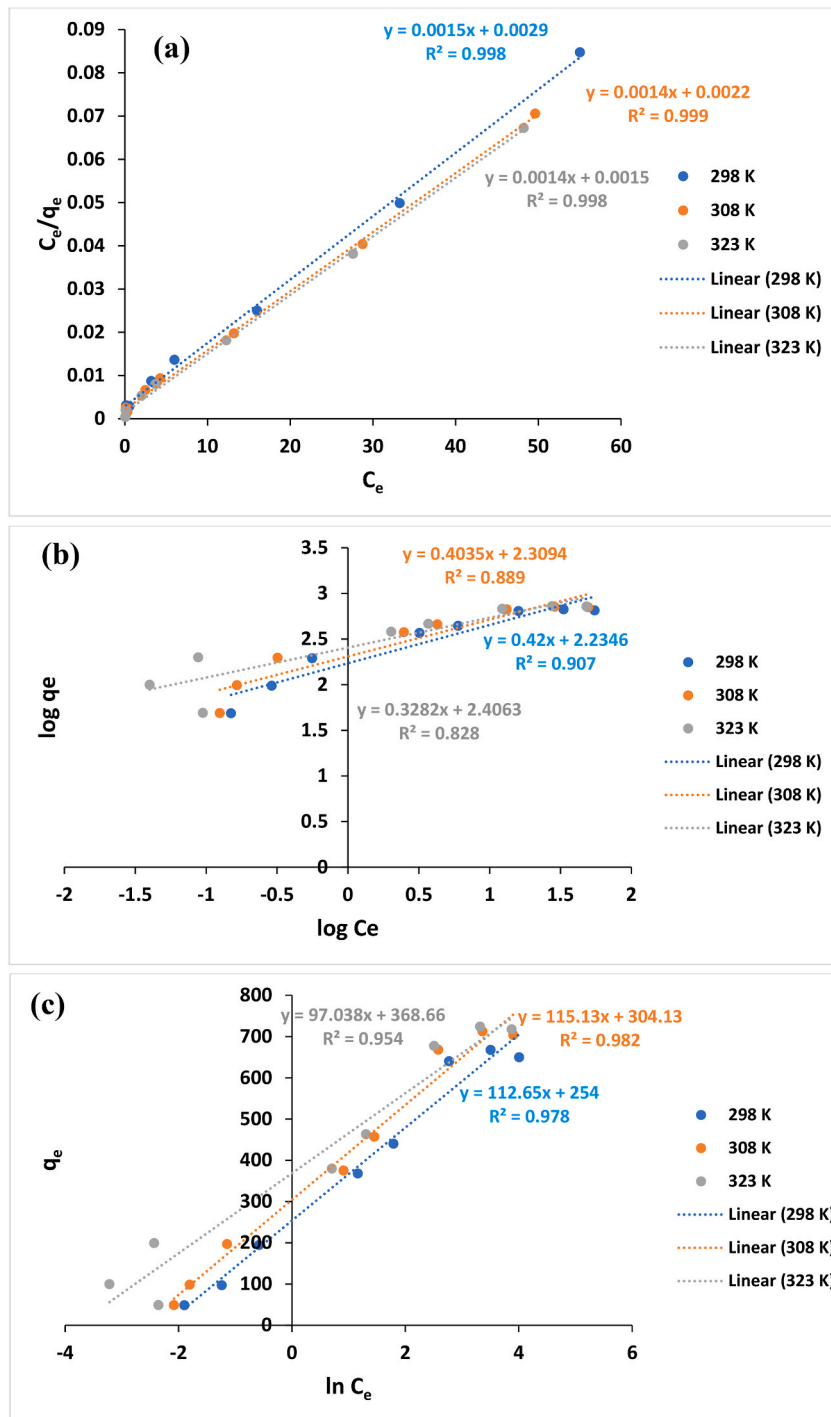


Fig. 4. Depictions of linearized isotherm models: Langmuir (a), Freundlich (b), and Temkin (c) for the process of As(III) adsorption onto TFPO/TDB-SO₃H.

(Eq. (5)) were utilized to understand the kinetics of the adsorption process. Eqs. (3)–(5) representing these models are as follows:

$$\ln(q_e - q_l) = \ln q_e - k_1 t \tag{3}$$

$$\frac{t}{q_t} = \frac{1}{k_2 q_e^2} + \frac{t}{q_e} \tag{4}$$

Table 1Assessing the adsorption isotherms of As(III) ions on TFPOADB-SO₃H: a comparative study of Langmuir, Freundlich, and Temkin models.

T (K)	Langmuir			R ²	Freundlich			Temkin		
	q _m (mg/g)	K _L (L/mg)	R _L ^a range		K _F [(mg/g) (L/mg) ^{1/n}]	1/n	R ²	A _T (L/g)	b _T (J/mol)	R ²
298	344.83	1.933	0.0938–0.0043	0.998	171.633	0.420	0.907	9.533	21.994	0.978
308	454.55	1.571	0.1129–0.0053	0.999	203.892	0.404	0.889	14.036	22.242	0.982
323	666.67	1.071	0.1574–0.0077	0.998	254.859	0.328	0.828	44.662	27.674	0.954

^a Initial concentrations of As(III) ions varied between 5 and 120 mg/L.

$$q_t = \frac{1}{\beta} \ln(\alpha\beta) + \left(\frac{1}{\beta}\right) \ln t \quad (5)$$

The model of pseudo-first order incorporates elements like q_e (mg/g) and q_t (mg/g). These represent the ability to adsorb As(III) ions when in equilibrium and at a specific time t (min), respectively. The reaction speed is dictated by the rate coefficient of the quasi-first order reaction, symbolized as k₁ (min⁻¹). In the quasi-second-order model, the terms q_e (mg/g) and q_t (mg/g) are used to represent the steady-state and time-variant uptake capacity of As(III) ions, respectively. The speed coefficient for this quasi-second-order reaction is represented as k₂ (g/mg.min). In the context of the Elovich model, the symbols α (mg/g.min) and β (g/mg) are used to denote the initial rate of adsorption and a constant that provides details about the extent of surface coverage, respectively.

The outcomes of the fitting analysis can be found in Table S1 and Fig. S2. The pseudo-second-order model appears to be the most suitable for characterizing the adsorption process, as indicated by the R² values. This implies that chemisorption, which includes ion exchange and coordination between As(III) ions and the sorbent, could be the step that most influences the rate of As(III) ions adsorption onto TFPOADB-SO₃H.

3.6. As(III) adsorption isotherms

The equilibrium distribution of adsorbate molecules between the solid and liquid phases can be assessed by conducting adsorption isotherm studies. In this study, the Langmuir, Freundlich, and Temkin isotherm models were employed to analyze the results obtained from the isotherm experiments (Fig. 4). Eqs. (6)–(8) represent the linear forms of the Langmuir, Freundlich and Temkin adsorption isotherm equations, respectively:

$$\frac{C_e}{q_e} = \frac{1}{K_L q_m} + \frac{C_e}{q_m} \quad (6)$$

$$\log q_e = \log K_F + \frac{1}{n} \log C_e \quad (7)$$

$$q_e = \frac{RT}{b_T} \ln A_T + \frac{RT}{b_T} \ln C_e \quad (8)$$

The equations are composed of several signs and coefficients. The equilibration concentration of As(III) is C_e (mg/L), and the quantity of arsenic sorbed at equilibrium is q_e (mg/g). The constant for the Langmuir isotherm is K_L (L/mg), and the constants for the Freundlich isotherm are K_F [(mg/g) (L/mg)^{1/n}] and 1/n. The equilibrium binding coefficient, and the heat of adsorption are related to the Temkin isotherm constants, A_T and b_T, respectively, and their units are L/g. The global gas constant is R, which is 8.314 J/mol-K, and the temperature in Kelvin is T. The adsorption is favorable if the amount of n from the computations is more than 1. On the other hand, the adsorption is irreversible if the value of n is 0 [50].

The isotherm models' related elements and their regression factor (R²) are briefed in Table 1 and can be derived from the relevant charts (Fig. 4 (a–c)), as described. The appropriateness of the model can be evaluated by contrasting the R² amounts of various models. A superior R² signifies a more fitting model. The findings in Table 1 show that the Langmuir model has a higher R² than the Freundlich and Temkin models at various temperatures. This implies that the Langmuir model offers a superior characterization of the impact of As(III) uptake on adsorbent. Additionally, it indicates that the uptake of As(III) on adsorbent adheres to a monolayer uptake process [51,52]. At the outset, the TFPOADB-SO₃H's surface locations with the greatest energy are filled. The finding is supported by the Langmuir isotherm, which supposes an equal surface with the same uptake sites, no interaction between adsorbed particles, and a one-layer formation at utmost uptake. When a location is occupied, no further adsorbates can attach to that spot, leading to saturation and utmost uptake on the surface [53,54]. The formula $R_L = \frac{1}{1+K_L C_0}$ establishes the dimensionless factor R_L, where its magnitude represents the adsorption traits. An R_L value from 0 to 1 denotes suitable adsorption, R_L exceeding 1 implies unsuitable adsorption, and R_L equating to 0 signifies unalterable adsorption [55]. In the current research, the observed R_L values varied between 0.1574 and 0.0043, signifying the efficient adsorption of As(III) onto the TFPOADB-SO₃H substance. To test whether TFPOADB-SO₃ is also effective at low concentrations, we utilized an extremely minimal concentration of 10 μg/L, which is the World Health Organization's limit for As(III) in drinking water. Remarkably, even with an adsorbent concentration of just 0.01 g/100 mL, TFPOADB-SO₃H demonstrated an impressive capability by removing 96.3 % of As(III) and reducing the final concentration to 0.37 μg/L. The TFPOADB-SO₃H exhibits impressive performance in relation to its adsorption capability for As(III) ions. This is probably attributable to

the plentiful presence of sulfonic acid groups and N, O atoms on the TFPOTDB-SO₃H framework, which amplifies the density of coordination locations ion and exchange, resulting in a substantial metal-loading capacity and affinity.

3.7. As(III) adsorption thermodynamics

The uptake capacity of an adsorbent is greatly influenced by the temperature. The absorption of As(III) ions by TFPOTDB-SO₃H was examined at various temperatures, from 298 to 323 K. The study found that with an increase in temperature, there was a corresponding increase in adsorption, suggesting that the uptake process is heat-absorbing. This finding agrees with previous studies [56–58] (Fig. S3). To evaluate the practicality and comprehend the uptake mechanism, the thermodynamical variables such as change in enthalpy (ΔH), change in free energy (ΔG), and change in entropy (ΔS) were scrutinized. The calculations for ΔH and ΔS were performed using the gradients and y-intercepts obtained from the graphs of $\ln K_c$ against $1/T$ (refer to Fig. S4), utilizing the corresponding formulas (9–11).

$$\ln(K_c) = \ln\left(\frac{q_e}{C_e}\right) = \frac{-\Delta G}{RT} \quad (9)$$

$$\ln(K_c) = \frac{-\Delta H}{RT} + \frac{\Delta S}{R} \quad (10)$$

$$\Delta G = \Delta H - T\Delta S \quad (11)$$

The ratio of q_e/C_e determines the thermodynamic constant K_c (L/mg), where R (8.314 kJ/mol.K) is the gas constant and T (K) is the absolute temperature. The quantities of ΔG , ΔH and ΔS for the adsorption of As(III) onto the adsorbent are presented in Table S2. The positive value of ΔH indicates an endothermic character to the adsorption process. The ΔH value provides interesting information about the type of adsorption process. Table S2 shows that the adsorption of As(III) onto TFPOTDB-SO₃H has an ΔH value of 65.129 kJ/mol, indicating a certain percentage of chemical adsorption [59]. The entropy changes (ΔS) with positive values indicate that there is an increase in disorder at the solid/liquid interface in agreement with the adsorption of As(III). Additionally, the negative ΔG values obtained indicate that the adsorption process is spontaneous and feasible within the studied temperature range.

3.8. Analyzing the selectivity of arsenic adsorption

In practical scenarios, the presence of other species poses a significant challenge to the adsorption performance of the adsorbent. It has been established that phosphates can interfere with the adsorption of As(III) [60]. To further explore this concept, an experiment was conducted using anions such as PO_4^{3-} , Cl^- , SiO_3^{2-} , and SO_4^{2-} . Results showed that only PO_4^{3-} had a significant effect on the removal of As(III) in water, decreasing the uptake to 90.5 % (Fig. S5).

3.9. Examining the humic acid on As(III) adsorption

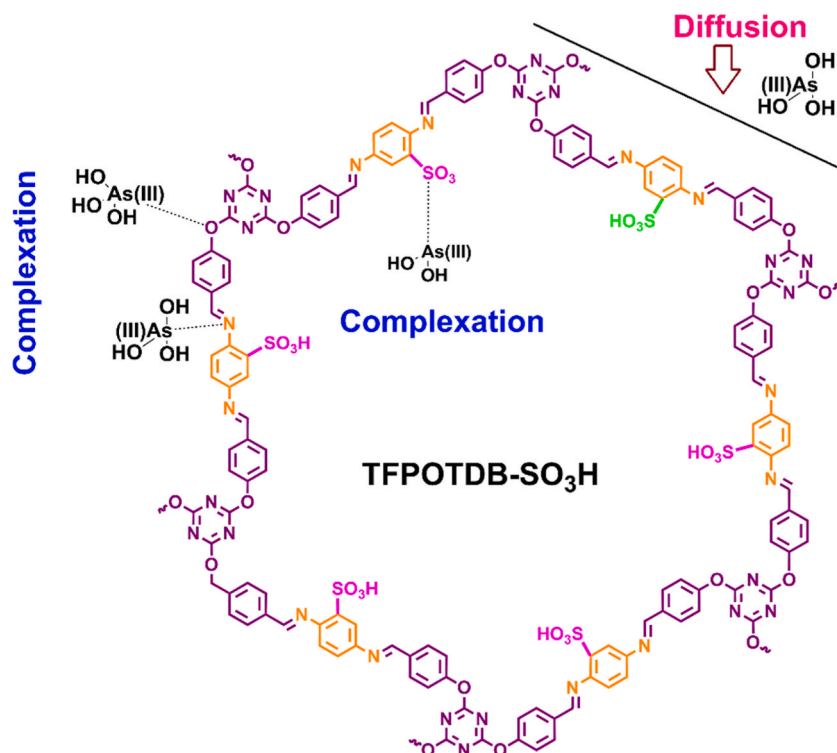
Our research focused on the impact of humic acid (HA), a crucial natural organic compound, on the As(III) adsorption by TFPOTDB-SO₃H. As depicted in Fig. S6, varying quantities of HA had distinct influences on the TFPOTDB-SO₃H's adsorption ability. When the HA concentration was 5 mg/L, it enhanced the TFPOTDB-SO₃H's As(III) adsorption, but when the concentration increased to 10 mg/L, it hindered the process. Previous researches indicated that an abundance of negatively charged HA molecules could vie with As(III) for active adsorption sites [61,62]. Consequently, introducing high concentrations of HA diminished the TFPOTDB-SO₃H's As(III) adsorption capacity. This is primarily because low concentrations of HA allow TFPOTDB-SO₃H to offer more adsorption sites, and there is no competitive adsorption between HA and As(III). The introduction of HA might also alter the solution's pH, thereby augmenting the quantity of adsorption. However, when the HA quantity is elevated to a certain level, it begins to compete with As(III) for adsorption, which impacts the TFPOTDB-SO₃H's As(III) adsorption efficacy.

3.10. Investigating the effectiveness of the TFPOTDB-SO₃H on As(III) adsorption in tap water

The effect of some common ions on the adsorption process of As(III) was investigated in previous experiments. Since all ions are present in real environments such as tap water, it is necessary to check the performance of the adsorbent in the real environment. For this purpose, the adsorption capacity for a volume of 100 mL tap water containing a concentration of 10 mg/L As(III) at pH = 8 was investigated. The temperature was set at 25 °C. After stabilizing the temperature, 10 mg of TFPOTDB-SO₃H was added to the solution and C_e was measured according to the procedure in Section 2.5 and the adsorption capacity were calculated. The obtained results show that the efficiency of the TFPOTDB-SO₃H in the real environment is lower than that of distilled water (Fig. S7). In the real environment, due to the effect of ions in tap water on the As(III) adsorption, the removal efficiency and adsorption capacity of the TFPOTDB-SO₃H decreased slightly.

3.11. Arsenic adsorption mechanism

The research into the adsorption of As(III) onto TFPOTDB-SO₃H considers the influence of pH and pHzpc. It was found that the



Scheme 2. The adsorption process of As(III) by TFPOTDB-SO₃H and its probable mechanism.

Table 2

Evaluating the maximum adsorption capacities of As(III) using various adsorbents.

Adsorbent	Langmuir adsorption capacity q_m (mg/g)	References
DU66	204.2	[49]
γ -Fe ₂ O ₃ @CTF-1	198.0	[64]
Fe/Mn bimetallic MOF	138.0	[65]
MOF-74(Zn)	211.0	[66]
Iron Oxyhydroxide-COF	272.0	[4]
Fe ₃ O ₄ @TA@UiO-66	97.8	[67]
Zirconia nanostructures	105.0	[68]
TFPOTDB-SO ₃ H	344.8	This study

greatest removal rate was at pH 8, where electrostatic attraction is not possible because the adsorbent is negatively charged (pHpzc = 3.42), and arsenic is neutral H₃AsO₃. Instead, as depicted in [Scheme 2](#), the adsorption is thought to be mainly caused by complexation between surface functional groups (–C=N, –SO₃ and C–O) on TFPOTDB-SO₃H and H₃AsO₃, diffusion, van der Waals forces and hydrogen bonding at pH 3–8. This trend has been seen previously [[46,48,63](#)].

3.12. Assessments of performance

The maximum adsorption capacity of As(III) by the TFPOTDB-SO₃H was compared to other adsorbents mentioned in [Table 2](#). The TFPOTDB-SO₃H's high porosity, which results in a large surface area for As(III) adsorption, indicates its significant advantages. This is attributed to its high adsorption capacity of 344.83 mg/g at 298 K and rapid removal within 10 min. Consequently, the TFPOTDB-SO₃H nano adsorbent shows promise as an effective and selective solution for removing As(III).

4. Conclusion

COFs are notably effective in the eradication of heavy metals, a capability that stems from their distinct properties such as their considerable porosity, enduring stability, expansive surface area, and an abundance of readily available active locations. To summarize, this research demonstrates an easy method for synthesizing TFPOTDB-SO₃H as a potent adsorbent to remove As(III) ions from aquatic environments. The structure and composition of TFPOTDB-SO₃H were examined using various analytical techniques.

Experimental tests revealed that the optimal adsorption occurred at pH 8, contact time: 10 min and adsorbent dosage: 10 mg for As(III) ions. The adsorption behavior of As(III) ions onto TFPOTDB-SO₃H followed the Langmuir isotherm model and the pseudo-second order model, describing monolayer adsorption on the sorbent surface with a maximum adsorption capacity of 344.8 mg/g at 298 K. Thermodynamic analysis indicated that the adsorption process was spontaneous and endothermic. Complete desorption of adsorbed As(III) ions was achieved using 5 M NaCl. Reusability investigations demonstrated that TFPOTDB-SO₃H maintained over 88 % of its initial efficiency after 4 cycles. These findings highlight that the TFPOTDB-SO₃H COF has shown itself to be a potent, cost-effective, and environmentally friendly adsorbent. It offers additional advantages such as simple manufacturing processes and zero by-product creation. As such, it presents a promising solution for mitigating environmental pollution.

Data availability statement

Data will be made available on request.

CRediT authorship contribution statement

Mohammad Khosravani: Visualization, Software, Investigation, Data curation. **Mohsen Dehghani Ghanatghestani:** Writing – review & editing, Supervision, Conceptualization. **Farid Moeinpour:** Writing – review & editing, Writing – original draft, Supervision, Methodology, Data curation. **Hossein Parvareh:** Writing – review & editing, Validation, Software, Methodology, Conceptualization.

Declaration of competing interest

The authors declare that they have no known competing financial interests or personal relationships that could have appeared to influence the work reported in this paper.

Acknowledgements

Special thanks are extended to the Islamic Azad University Bandar Abbas Branch for its partial financial support.

Appendix A. Supplementary data

Supplementary data to this article can be found online at <https://doi.org/10.1016/j.heliyon.2024.e25423>.

References

- [1] P.H. Gleick, Global freshwater resources: soft-path solutions for the 21st century, *Science* 302 (5650) (2003) 1524–1528.
- [2] A. Luch, *Molecular, Clinical and Environmental Toxicology: Volume 3: Environmental Toxicology*, vol. 101, Springer Science & Business Media, 2012.
- [3] M.A. Shannon, et al., Science and technology for water purification in the coming decades, *Nature* 452 (7185) (2008) 301–310.
- [4] A. Guillem-Navajas, et al., Iron oxyhydroxide-covalent organic framework nanocomposite for efficient as (III) removal in water, *ACS Appl. Mater. Interfaces* 14 (44) (2022) 50163–50170.
- [5] N.A. Qasem, R.H. Mohammed, D.U. Lawal, Removal of heavy metal ions from wastewater: a comprehensive and critical review, *NPJ Clean Water* 4 (1) (2021) 36.
- [6] L. Hao, M. Liu, N. Wang, G. Li, A critical review on arsenic removal from water using iron-based adsorbents, *RSC Adv.* 8 (69) (2018) 39545–39560.
- [7] D. Mohan, C.U. Pittman Jr., Arsenic removal from water/wastewater using adsorbents—a critical review, *J. Hazard Mater.* 142 (1–2) (2007) 1–53.
- [8] A. Majumder, et al., Green synthesis of iron oxide nanoparticles for arsenic remediation in water and sludge utilization, *Clean Technol. Environ. Policy* 21 (2019) 795–813.
- [9] S.R. Kanel, B. Manning, L. Charlet, H. Choi, Removal of arsenic (III) from groundwater by nanoscale zero-valent iron, *Environ. Sci. Technol.* 39 (5) (2005) 1291–1298.
- [10] R. Xu, et al., Hierarchically porous UiO-66 with tunable mesopores and oxygen vacancies for enhanced arsenic removal, *J. Mater. Chem. A* 8 (16) (2020) 7870–7879.
- [11] N. Assaad, G. Sabeh, M. Hmadeh, Defect control in Zr-based metal–organic framework nanoparticles for arsenic removal from water, *ACS Appl. Nano Mater.* 3 (9) (2020) 8997–9008.
- [12] A.M. Yusof, N.A.N.N. Malek, Removal of Cr (VI) and as (V) from aqueous solutions by HDTMA-modified zeolite Y, *J. Hazard Mater.* 162 (2–3) (2009) 1019–1024.
- [13] X.-Y. Yu, et al., Porous hierarchically micro-/nanostructured MgO: morphology control and their excellent performance in as (III) and as (V) removal, *J. Phys. Chem. C* 115 (45) (2011) 22242–22250.
- [14] Y. Liu, Q. Li, S. Gao, J.K. Shang, Exceptional as (III) sorption capacity by highly porous magnesium oxide nanoflakes made from hydrothermal synthesis, *J. Am. Ceram. Soc.* 94 (1) (2011) 217–223.
- [15] L. Cumbal, A.K. SenGupta, Arsenic removal using polymer-supported hydrated iron (III) oxide nanoparticles: role of Donnan membrane effect, *Environ. Sci. Technol.* 39 (17) (2005) 6508–6515.
- [16] E.A. Gendy, et al., Removal of heavy metals by covalent organic frameworks (COFs): a review on its mechanism and adsorption properties, *J. Environ. Chem. Eng.* 9 (4) (2021) 105687.
- [17] J. Wang, S. Zhuang, Covalent organic frameworks (COFs) for environmental applications, *Coord. Chem. Rev.* 400 (2019) 213046.
- [18] X. Feng, X. Ding, D. Jiang, Covalent organic frameworks, *Chem. Soc. Rev.* 41 (18) (2012) 6010–6022.
- [19] S. Kandambeth, et al., Construction of crystalline 2D covalent organic frameworks with remarkable chemical (acid/base) stability via a combined reversible and irreversible route, *J. Am. Chem. Soc.* 134 (48) (2012) 19524–19527.

- [20] B.J. Smith, W.R. Dichtel, Mechanistic studies of two-dimensional covalent organic frameworks rapidly polymerized from initially homogenous conditions, *J. Am. Chem. Soc.* 136 (24) (2014) 8783–8789.
- [21] M. Dinari, M. Hatami, Novel N-riched crystalline covalent organic framework as a highly porous adsorbent for effective cadmium removal, *J. Environ. Chem. Eng.* 7 (1) (2019) 102907.
- [22] C. Tang, Y. Qin, C. Ni, J. Zou, Detection and removal of mercury ions in water by a covalent organic framework rich in sulfur and nitrogen, *ACS Appl. Polym. Mater.* 4 (2) (2022) 849–858.
- [23] A. Khojastehnezhad, et al., Postsynthetic modification of core-shell magnetic covalent organic frameworks for the selective removal of mercury, *ACS Appl. Mater. Interfaces* 15 (2023) 28476–28490.
- [24] K. Li, et al., Synergistic effect of functionalization and crystallinity in nanoporous organic frameworks for effective removal of metal ions from aqueous solution, *ACS Appl. Nano Mater.* 5 (10) (2022) 15228–15236.
- [25] J. Gan, et al., Covalent organic frameworks-based smart materials for mitigation of pharmaceutical pollutants from aqueous solution, *Chemosphere* 286 (2022) 131710.
- [26] R. Zhu, et al., Fabrication of synergistic sites on an oxygen-rich covalent organic framework for efficient removal of Cd (II) and Pb (II) from water, *J. Hazard Mater.* 424 (2022) 127301.
- [27] J. Yang, L. Huang, J. You, Y. Yamauchi, Magnetic covalent organic framework composites for wastewater remediation, *Small* (2023) 2301044.
- [28] L. Huang, R. Shen, R. Liu, Q. Shuai, Thiol-functionalized magnetic covalent organic frameworks by a cutting strategy for efficient removal of Hg²⁺ from water, *J. Hazard Mater.* 392 (2020) 122320.
- [29] R. Liu, et al., Microenvironment engineering of covalent organic frameworks for the efficient removal of sulfamerazine from aqueous solution, *J. Environ. Chem. Eng.* 10 (2) (2022) 107300.
- [30] M. Afshari, M. Dinari, H. Moradi, Z. Noori, Polyaniline/sulfonated-covalent organic polymer nanocomposite: structural and dye adsorption properties, *Polym. Adv. Technol.* 31 (11) (2020) 2433–2442.
- [31] N. Mokhtari, et al., Imine-based covalent triazine framework: synthesis, characterization, and evaluation its adsorption, *Mater. Lett.* 263 (2020) 127221.
- [32] N. Anahidzade, et al., Metal-organic framework anchored sulfonated poly (ether sulfone) as a high temperature proton exchange membrane for fuel cells, *J. Membr. Sci.* 565 (2018) 281–292.
- [33] A. Wen, et al., Sulphonate functionalized covalent organic framework-based magnetic sorbent for effective solid phase extraction and determination of fluoroquinolones, *J. Chromatogr. A* 1612 (2020) 460651.
- [34] W. Zhao, et al., Evaluation of sulfonic acid functionalized covalent triazine framework as a hydrophilic-lipophilic balance/cation-exchange mixed-mode sorbent for extraction of benzimidazole fungicides in vegetables, fruits and juices, *J. Chromatogr. A* 1618 (2020) 460847.
- [35] T.K. Dutta, A. Patra, Post-synthetic modification of covalent organic frameworks through in situ polymerization of aniline for enhanced capacitive energy storage, *Chem.-Asian J.* 16 (2) (2021) 158–164.
- [36] K. Jeong, et al., Solvent-free, single lithium-ion conducting covalent organic frameworks, *J. Am. Chem. Soc.* 141 (14) (2019) 5880–5885.
- [37] S. Chandra, et al., Interplaying intrinsic and extrinsic proton conductivities in covalent organic frameworks, *Chem. Mater.* 28 (5) (2016) 1489–1494.
- [38] P. Pachfule, et al., Diacetylene functionalized covalent organic framework (COF) for photocatalytic hydrogen generation, *J. Am. Chem. Soc.* 140 (4) (2018) 1423–1427.
- [39] Y. Zhao, et al., Facile grafting of imidazolium salt in covalent organic frameworks with enhanced catalytic activity for CO₂ fixation and the Knoevenagel reaction, *ACS Sustain. Chem. Eng.* 8 (50) (2020) 18413–18419.
- [40] S.S. Altarawneh, J.B. Max, F.H. Schacher, T.S. Ababneh, Synthesis, characterization, thermodynamics and thermal degradation kinetics of imine-linked polymers, *J. Polym. Res.* 27 (2020) 1–15.
- [41] X. Li, et al., Facile transformation of imine covalent organic frameworks into ultrastable crystalline porous aromatic frameworks, *Nat. Commun.* 9 (1) (2018) 2998.
- [42] F.J. Uribe-Romo, et al., A crystalline imine-linked 3-D porous covalent organic framework, *J. Am. Chem. Soc.* 131 (13) (2009) 4570–4571.
- [43] M.G. Rabbani, et al., A 2D mesoporous imine-linked covalent organic framework for high pressure gas storage applications, *Chem.-Eur. J.* 19 (10) (2013) 3324–3328.
- [44] W. Song, et al., Immobilization of as (V) in *Rhizopus oryzae* investigated by batch and XAFS techniques, *ACS Omega* 1 (5) (2016) 899–906.
- [45] V. Chandra, et al., Water-dispersible magnetite-reduced graphene oxide composites for arsenic removal, *ACS Nano* 4 (7) (2010) 3979–3986.
- [46] A.S.K. Kumar, S.-J. Jiang, Chitosan-functionalized graphene oxide: a novel adsorbent an efficient adsorption of arsenic from aqueous solution, *J. Environ. Chem. Eng.* 4 (2) (2016) 1698–1713.
- [47] Y. Yoon, et al., Comparative evaluation of magnetite-graphene oxide and magnetite-reduced graphene oxide composite for as (III) and as (V) removal, *J. Hazard Mater.* 304 (2016) 196–204.
- [48] A.A. Tabatabaiee Bafrooe, et al., Ethylenediamine functionalized magnetic graphene oxide (Fe₃O₄@GO-EDA) as an efficient adsorbent in Arsenic (III) decontamination from aqueous solution, *Res. Chem. Intermed.* 47 (2021) 1397–1428.
- [49] V. Somjit, et al., Hydroxylation of UiO-66 metal-organic frameworks for high arsenic (III) removal efficiency, *Inorg. Chem.* 61 (29) (2022) 11342–11348.
- [50] T.A. Arica, E. Ayas, M.Y. Arica, Magnetic MCM-41 silica particles grafted with poly (glycidylmethacrylate) brush: modification and application for removal of direct dyes, *Microporous Mesoporous Mater.* 243 (2017) 164–175.
- [51] X. Min, et al., Ultra-high capacity of lanthanum-doped UiO-66 for phosphate capture: unusual doping of lanthanum by the reduction of coordination number, *Chem. Eng. J.* 358 (2019) 321–330.
- [52] F. Omidvar-Hosseini, F. Moeinpour, Removal of Pb (II) from aqueous solutions using Acacia Nilotica seed shell ash supported NiO. 5ZnO. 5Fe₂O₄ magnetic nanoparticles, *J. Water Reuse Desalination* 6 (4) (2016) 562–573.
- [53] P. Beigzadeh, F. Moeinpour, Fast and efficient removal of silver (I) from aqueous solutions using aloe vera shell ash supported NiO. 5ZnO. 5Fe₂O₄ magnetic nanoparticles, *Trans. Nonferrous Metals Soc. China* 26 (8) (2016) 2238–2246.
- [54] M. Heidari-Chaleshtori, A. Nezamzadeh-Ejehie, Clinoptilolite nano-particles modified with aspartic acid for removal of Cu (II) from aqueous solutions: isotherms and kinetic aspects, *New J. Chem.* 39 (12) (2015) 9396–9406.
- [55] E. Zandi-Mehri, et al., Designing of hydroxyl terminated triazine-based dendritic polymer/halloysite nanotube as an efficient nano-adsorbent for the rapid removal of Pb (II) from aqueous media, *J. Mol. Liq.* 360 (2022) 119407.
- [56] H. Shan, et al., As (III) removal by a recyclable granular adsorbent through doping Fe-Mn binary oxides into graphene oxide chitosan, *Int. J. Biol. Macromol.* 237 (2023) 124184.
- [57] P. Zein Al-Salehin, F. Moeinpour, F.S. Mohseni-Shahri, Adsorption isotherm and thermodynamic studies of as (III) removal from aqueous solutions using used cigarette filter ash, *Appl. Water Sci.* 9 (8) (2019) 172.
- [58] N. Sahu, J. Singh, J.R. Koduru, Removal of arsenic from aqueous solution by novel iron and iron-zirconium modified activated carbon derived from chemical carbonization of *Tectona grandis* sawdust: isotherm, kinetic, thermodynamic and breakthrough curve modelling, *Environ. Res.* 200 (2021) 111431.
- [59] C.P. Okoli, et al., Aqueous scavenging of polycyclic aromatic hydrocarbons using epichlorohydrin, 1, 6-hexamethylene diisocyanate and 4, 4-methylene diphenyl diisocyanate modified starch: pollution remediation approach, *Arab. J. Chem.* 12 (8) (2019) 2760–2773.
- [60] C. Sudhakar, et al., Interference of phosphate in adsorption of arsenate and arsenite over confined metastable two-line ferrihydrite and magnetite, *J. Phys. Chem. C* 125 (41) (2021) 22502–22512.
- [61] E. Lorenc-Grabowska, G. Gryglewicz, Adsorption of lignite-derived humic acids on coal-based mesoporous activated carbons, *J. Colloid Interface Sci.* 284 (2) (2005) 416–423.
- [62] X. Liu, et al., Fe-Mn-Ce oxide-modified biochar composites as efficient adsorbents for removing as (III) from water: adsorption performance and mechanisms, *Environ. Sci. Pollut. Control Ser.* 26 (17) (2019) 17373–17382.

- [63] A. Sherlala, A. Raman, M.M. Bello, A. Buthiyappan, Adsorption of arsenic using chitosan magnetic graphene oxide nanocomposite, *J. Environ. Manag.* 246 (2019) 547–556.
- [64] K. Leus, et al., Removal of arsenic and mercury species from water by covalent triazine framework encapsulated γ -Fe₂O₃ nanoparticles, *J. Hazard Mater.* 353 (2018) 312–319.
- [65] T. Zhang, et al., Amorphous Fe/Mn bimetal–organic frameworks: outer and inner structural designs for efficient arsenic (iii) removal, *J. Mater. Chem. A* 7 (6) (2019) 2845–2854.
- [66] W. Yu, et al., Metal-organic framework (MOF) showing both ultrahigh as (V) and as (III) removal from aqueous solution, *J. Solid State Chem.* 269 (2019) 264–270.
- [67] P. Qi, et al., Development of a magnetic core-shell Fe₃O₄@ TA@ UiO-66 microsphere for removal of arsenic (III) and antimony (III) from aqueous solution, *J. Hazard Mater.* 378 (2019) 120721.
- [68] K. Shehzad, et al., Mesoporous zirconia nanostructures (MZN) for adsorption of as (III) and as (V) from aqueous solutions, *J. Hazard Mater.* 373 (2019) 75–84.